Acta Oceanol. Sin., 2022, Vol. 41, No. 1, P. 50–57
https://doi.org/10.1007/s13131-021-1979-8
http://www.aosocean.com
E-mail: ocean2@hyxb.org.cn

Crustal structure and variation along the southern part of the Kyushu-Palau Ridge

Xiaodong Wei[1, 2], Weiwei Ding[1, 2, 3*], Aiguo Ruan[1, 2, 3*], Jie Zhang[1, 2], Xiongwei Niu[1, 2], Jiabiao Li[1, 2, 3], Yong Tang[1, 2, 3]

[1] Key Laboratory of Submarine Geosciences, Ministry of Natural Resources/Second Institute of Oceanography, Ministry of Natural Resources, Hangzhou 310012, China

[2] Southern Marine Science and Engineering Guangdong Laboratory (Zhuhai), Zhuhai 519080, China

[3] School of Oceanography, Shanghai Jiao Tong University, Shanghai 200240, China

Received 30 November 2021; accepted 16 December 2021

Abstract

As an interoceanic arc, the Kyushu-Palau Ridge (KPR) is an exceptional place to study the subduction process and related magmatism through its interior velocity structure. However, the crustal structure and its nature of the KPR, especially the southern part with limited seismic data, are still in mystery. In order to unveil the crustal structure of the southern part of the KPR, this study uses deep reflection/refraction seismic data recorded by 24 ocean bottom seismometers to reconstruct a detailed P-wave velocity model along the ridge. Results show strong along-ridge variations either on the crustal velocity or the thickness of the KPR. P-wave velocity model is featured with (1) a crustal thickness between 6–12 km, with velocity increases from 4.0 km/s to 7.0 km/s from top to bottom; (2) high gradient (~1 s^{-1}) in the upper crust but low one (<0.2 s^{-1}) in the lower crust; (3) a slow mantle velocity between 7.2 km/s and 7.6 km/s in the uppermost mantle; and (4) inhomogenous velocity anomalies in the lower crust beneath seamounts. By comparing with the mature arc in the Izu-Bonin-Mariana arc in the east, this study suggests the southern part of KPR is a thicken oceanic crust rather than a typical arc crust. The origin of low velocities in the lower crust and upper mantle may be related with crustal differentiation, which implies advanced crustal evolution from normal oceanic crust to partly thicken oceanic crust. High velocities in the lower crust are related to the difference in magmatism.

Key words: P-wave velocity structure, ocean bottom seismometer, Kyushu-Palau Ridge, magmatism, thicken oceanic crust

Citation: Wei Xiaodong, Ding Weiwei, Ruan Aiguo, Zhang Jie, Niu Xiongwei, Li Jiabiao, Tang Yong. 2022. Crustal structure and variation along the southern part of the Kyushu-Palau Ridge. Acta Oceanologica Sinica, 41(1): 50–57, doi: 10.1007/s13131-021-1979-8

1 Introduction

As a typical case of convergent plate margin, the Izu-Bonin-Maria (IBM) subduction system is an ideal place to study the subduction factory due to the intensive lithospheric deformation and magmatism, arc splitting and back-arc spreading, and classic arc-trench-basin system (Cosca et al., 1998; Takahashi et al., 2008; Ishizuka et al., 2011). The Kyushu-Palau Ridge (KPR), initially formed with the subduction of the proto-Pacific plate beneath the West Philippine Sea plate, connected with the present IBM arc before the splitting of the proto-IBM arc and following back-arc spreading occurred in the Shikoku and Parece Vela Basins (Okino et al., 1998; Ishizuka et al., 2011, 2018). As a remnant oceanic arc, studies on the KPR could improve the understanding of the tectono-magmatic process during subduction, as well as the crustal evolution.

Wide-angle seismic experiment with ocean bottom seismometers (OBSs) is a useful method to map crustal structures and clarify the possible magmatic features of the basement (Korenaga et al., 2000; Kodaira et al., 2007b; Takahashi et al., 2009; Wei et al., 2021). Based on four wide-angle seismic profiles crossing the KPR between 15°N and 21°N, Nishizawa et al. (2007) presented an 8–20 km thick crust, which is generally thicker than the normal oceanic crust. Nishizawa et al. (2016) exhibited more detailed crustal structures with 27 OBS profiles crossing the KPR between 13°N and 35°N. They argued that the middle crust is much thicker compared with the IBM arc with a P-wave velocity between 6.0 km/s and 6.8 km/s, and the P-wave velocity in the lower crust is much higher (6.8–7.2 km/s). The crustal thickness is between 8 km and 23 km decreasing southward. However, the previous wide-angle seismic profiles are generally short (~180 km) and perpendicular to the KPR, and most of them distributed in the middle-northern part, which will hinder the understanding of the crustal structure and magmatic activities of the whole KPR, as well as the along-ridge variation and dynamic mechanism.

This study presents the along-ridge crustal structure of the southern part of the KPR derived from a 300 km long wide-angle

Foundation item: The Scientific Research Fund of the Second Institute of Oceanography, MNR under contract No. QNYC1801; the National Natural Science Foundation of China under contract Nos 91858214, 41776053, 42025601, 42076047, 41890811 and 42006072; the National Program on Global Change and Air-Sea Interaction, Ministry of Natural Resources under contract No. GASI-02-PAC-DWZP02; the Innovation Group Project of Southern Marine Science and Engineering Guangdong Laboratory (Zhuhai) under contract No. 311020018.

*Corresponding author, E-mail: wwding@sio.org.cn; ruanag@sio.org.cn

seismic profile, named KPR2020-3 (Fig. 1). This study applied joint reflection and refraction seismic travel time inversion to construct P-wave velocity structure of the KPR. By characterizing the crustal architecture and velocity anomalies, this study used these results to constrain the Cenozoic crustal evolution of the southern KPR. Attempts were also applied for the crustal nature of the KPR by comparing the crustal structure with that of the mature arc crust (e.g., IBM arc) and normal oceanic crust.

2 Tectonic setting

The KPR is a bathymetric high, extending continuously in the N-S direction over a distance of ~2 600 km from off the Kyushu in the north to the Palau in the south. It separated the Philippine Sea Plate into two tectonic domains. The west domain is the West Philippine Basin, and the east is the IBM subduction system, including the Shikoku and Parece Vela Basins, Mariana Trough, western Mariana Ridge, Izu-Ogasawara-Mariana island arc, and Izu-Ogasawara-Mariana Trench (Fig. 1). The West Philippine Basin was originally a back-arc basin developed in the south of the equator, and the initial seafloor spreading of the West Philippine Sea occurred in the early Cenozoic with estimated ages of 58 Ma (Hilde and Lee, 1984), 55 Ma (Deschamps and Lallemand, 2002; Hall, 2002), or 52–51 Ma (Ishizuka et al., 2011). Then it experienced NW-ward movement and anticlockwise rotation (Hall, 2002). Since ~50 Ma BP, the paleo-Pacific began its subduction under the West Philippine Basin along a transform fault resulted from gravitational instability of oceanic lithosphere (Cosca et al., 1998; Ishizuka et al., 2011; Arculus et al., 2015; Stern and Gerya, 2018), or relic arcs (Leng and Gurnis, 2015). The IBM subduction system began its development with fore-arc spreading first (Stern, 2004; Stern and Gerya, 2018), the splitting of the IBM arc (Ishizuka et al., 2018), and the back-arc spreading of the Shikoku and Parece Vela Basins, and the Mariana Trough with continuous eastward retreatment of the paleo-Pacific subduction (Watts and Weissel, 1975; Okino et al., 1994; Yamazaki et al., 2003; Sdrolias and Müller, 2006).

The KPR is considered to be a remnant arc separated from the proto-IBM since back-arc spreading began in the Shikoku Basin and Parece Vela Basin (30–15 Ma BP, Okino et al., 1994) and the Parece Vela Basin (29–12 Ma BP, Okino et al., 1998). While the eastern part of the proto-IBM arc moves eastwards continuously with the roll-back of the Pacific subduction, and experiences episodic subduction-related magmatism before finally reaching the present position. Nowadays, the KPR moves northward to the Nankai Trough along with the NNW movement of the Philippine Sea Plate, and subducts beneath the Ryukyu Trench.

3 Seismic data acquisition and processing

The wide-angle seismic profile KPR2020-3 was acquired in January 2020, which is 300 km long along the southern part of the KPR. Twenty-six 4-component OBSs (three components and one hydrophone) were deployed at an interval of 10 km. The source for seismic data acquisition was an air gun array towed at ~10 m depth to produce a low-frequency source of 3–15 Hz. The active array was composed of four air guns with total volume of 8 000 cubic inches, and the shot interval was 250 m. 1 521 shots were fired along with the profile with 24 instruments recording readable data.

OBS data were corrected assuming a linear drift of the internal clock during the data-collected period, and the internal clock offsets were checked before and after deployments. The position of the instrument on seafloor was constrained by fitting the direct water-wave phases using the least-square method. After this

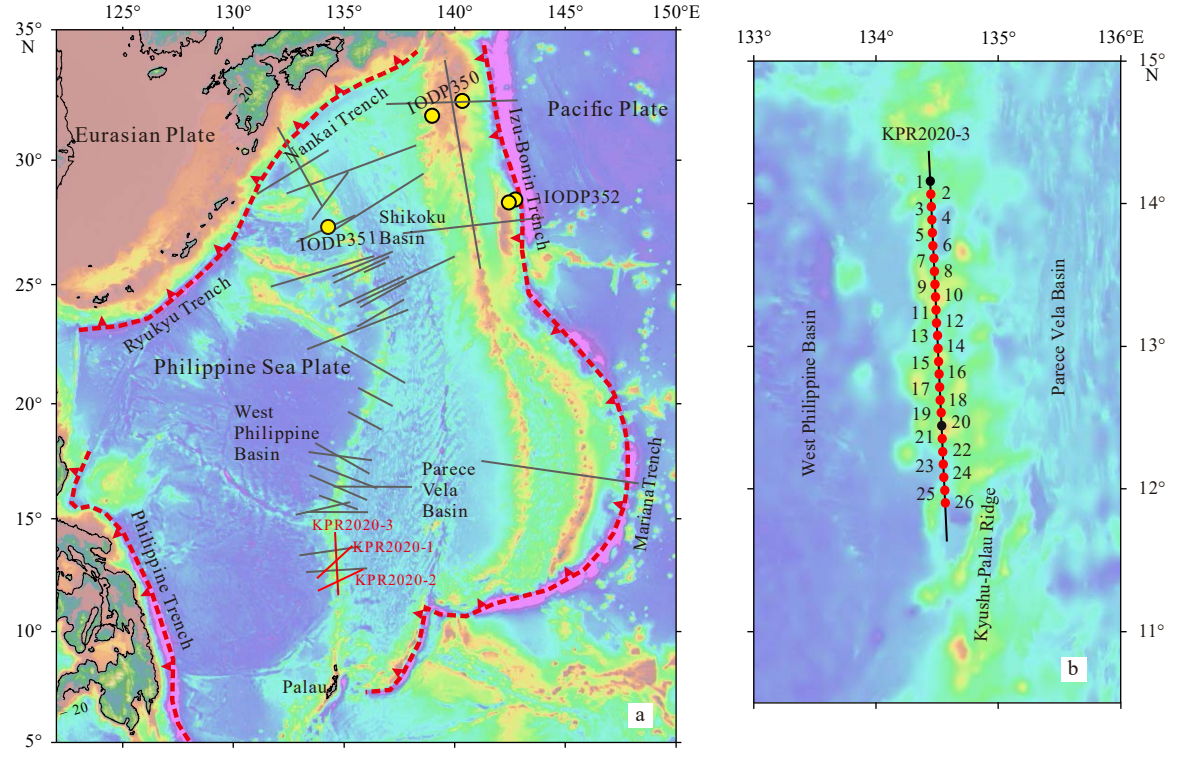

Fig. 1. Morphological features and major tectonic units in the study area. a. Bathymetric features of the KPR and adjacent area. b. Location of the wide-angle seismic profile KPR2020-3 in the KPR. Gray solid lines represent the previous OBS profiles acquired by Japan (Nishizawa et al., 2007, 2016); red dotted lines with triangles denote subduction zone around the study area; red solid lines represent OBS profiles acquired in 2020; red circles mark the OBSs used in this paper, while the black circles mark the invalid OBSs.

processing, the recorded OBS data were converted into the standard SEG-Y format and stored in the common received set. Further processing consisted of applying a Butterworth filter with a low cut of 3 Hz, a high cut of 15 Hz to enhance the signal-to-noise (S/N) ratios of some weak seismic phases, and a gain as a function of offset to optimize the picking at different offset ranges. The P-wave model was calculated from the hydrophone components of all the OBSs. By picking a series of phases, each single-receiver record was plotted with a reduced velocity of 8.0 km/s (Figs 2b and f).

4 Velocity modeling

4.1 *Identification of seismic phases*

All OBS data of KPR2020-3 are high quality and arrivals from the crust and upper mantle were identified in the vertical components. As the height varies greatly along the ridge, the seismic phases in the profile KPR2020-3 are affected severely by the bathymetry (Figs 2a and e). In order to identify and pick the phases precisely, a seafloor correction was carried out, i.e., the effects of the water column were deducted for the travel time of each shot of the OBS sections. During this calculation, this study assumed that the depth of each air gun propagating in water approximately corresponds to the vertical depth. After the seafloor correction, the seismic phases were relatively easy to identify by comparing the theoretical curves (Figs 2c and g). This study identified four types of seismic phases from the OBS profiles, named as Pw, Pg, PmP, and Pn, respectively. Pw and PmP are reflection phases, which represent the reflected waves from the seafloor and Moho, respectively. Pg and Pn are refraction phases, which denote the refracted waves from the crust and upper mantle, respectively. Figure 2 shows two examples of seismic records and phase identification, displaying clear reflected and refracted phases. Pg phases are clearly observable on all the OBSs sections and the offset is about 10–50 km with lateral variations resulted from the bathymetric features. PmP phases have a near-offset apparent velocity of 8.0 km/s, with the offset of 30–60 km is evident in most OBS records and easily recognized, which are used to constrain the Moho depth. Pn phases are identified on all the OBSs sections with the maximum offset of 100 km.

According to the kinematic and dynamic characteristics, a total of 8 356 arrivals including 746 PmP phases were picked. Based on S/N ratio using the empirical parameterization of Zelt and Forsyth (1994) and data qualities, the picking uncertainties were assigned from 30 ms to 100 ms. Generally, refracted phases at near offset were assigned low picking errors ranging in 30–60 ms, whereas phases from far offsets or disturbed by reverberation were assigned high values in 60–100 ms.

4.2 *Tomographic inversion*

P-wave velocity of profile KPR2020-3 was obtained using joint refraction and reflection travel time inversion code of Tomo2D

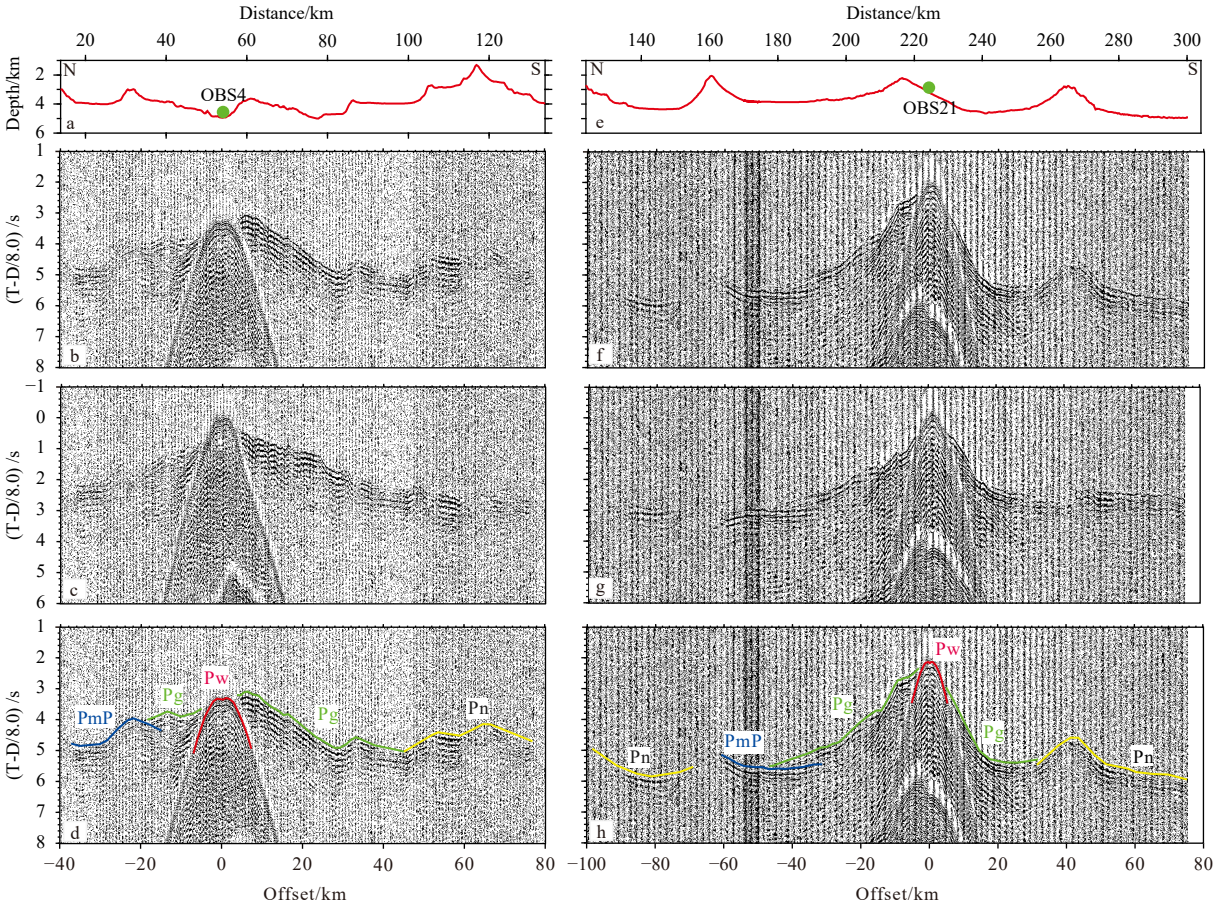

Fig. 2. Record sections and seismic phases identification of OBS4 (left) and OBS21 (right). a and e represent seafloor bathymetry and OBS positions; b and f represent the vertical component of the OBS4 and OBS21, respectively; c and g represent the seismic record section after a static shift corrected by the seafloor depth; d and h represent the seismic record sections with seismic phases identification. T-D represents vertical component data of OBS. In these diagrams, the reduction velocity is 8.0 km/s.

(Korenaga et al., 2000). The Tomo2D code allows simultaneous and independent inversion of the travel times from refracted and reflected phases, obtaining a velocity model and the geometry of the floating reflectors (Korenaga et al., 2000). The velocity model is parameterized as a sheared mesh hanging beneath the seafloor. It is then interpolated to form a continuous velocity field. The sheared mesh representation allows accurate travel time calculation by ray-bending and graph methods, while the velocity field is estimated based on the travel time residuals. Smoothing constraints for predefined correlation lengths and optimized damping for model parameters were used to regularize the iterative linearized inversion (Korenaga et al., 2000).

Although the initial model can be freely chosen in Tomo2D, this study conducted the one-dimensional (1D) initial velocity according to the precious velocity structure in this area. The initial velocity model below the seabed uniformly varied from 2.2 km/s to 8.2 km/s in the lower crust (Fig. 3a). The initial Moho reflector is set at a constant depth of 20 km. This study used Pg phases first to invert velocity of the upper crust, and then PmP and Pn phases were included for complete crust based on the previous inversions.

During the Tomo2D inversion, the model was parameterized with grid cells and a node spacing of 0.5 km×0.25 km, and the Moho was defined with a uniform of 1 km spacing. The final model used horizontal correlation lengths of 2 km and 8 km at the top and bottom, respectively. The vertical correlation length increased from 0.4 km to 5 km. This study applied a correlation length of 4 km for Moho reflectors. After nine iterations, the root mean square misfit of the crustal model had a convergence at 95 ms, and the final χ^2 value was 1.37; thus, the corresponding final velocity model was obtained (Fig. 3b).

4.3 *Model uncertainty*

This study conducted checkerboard tests to validate the reliability of the Tomo2D velocity models. This study imposed checkerboard patterns with a width of 10 km, a height of 8 km, and a velocity perturbation of ±5%. Based on these perturbed models, synthetic travel times were calculated using the same source-receiver geometry. After adding a random noise of 100 ms, the synthetic travel times were inverted for the output models (Fig. 4), based on the corresponding starting models that this study used in the inversion procedure. Checkerboard recovery is best in the sediments and crust (0–10 km); below the Moho, the resolution is better in the vertical than the horizontal direction. Resolution is poor at model edges where there is limited ray coverage. This study also computed the derivative weight sum (Fig. 3c), which was the column-sum vector of the Frechet velocity kernel and served as a measure of the linear sensitivity of the inversion. The derivative weight sum shows better coverage in the upper crust than the lower one.

4.4 *Modeling results*

The reflection and refraction seismic data in profile KPR2020-3 are crucial to reveal the crustal structure of the southern part of the KPR. The final velocity model indicates that major changes in crustal structure are accommodated by strong lateral variations

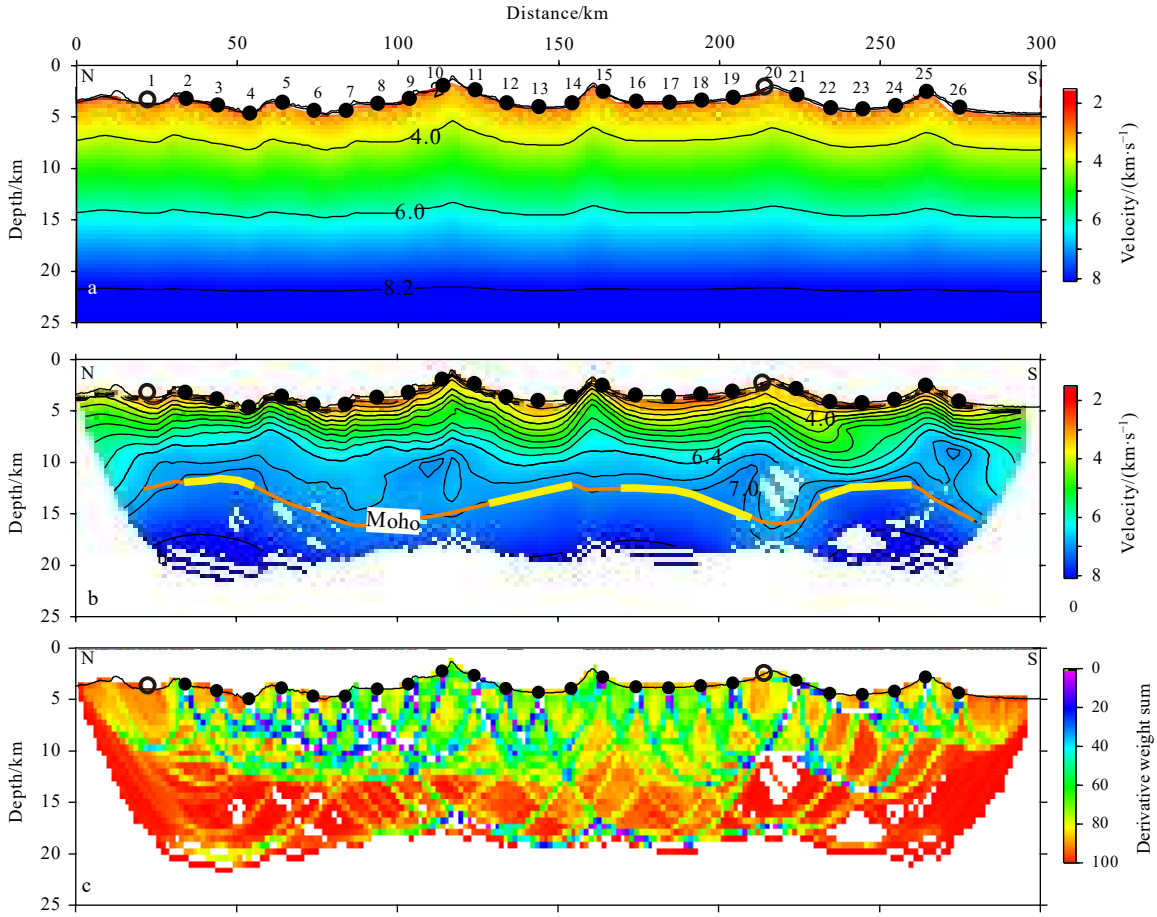

Fig. 3. Initial (a) and final (b) inversion-velocity model of profile KPR2020-3, and derivative weight sum for the final velocity model (c). In b, orange solid line is Moho, and the yellow lines are constrained by PmP phases.

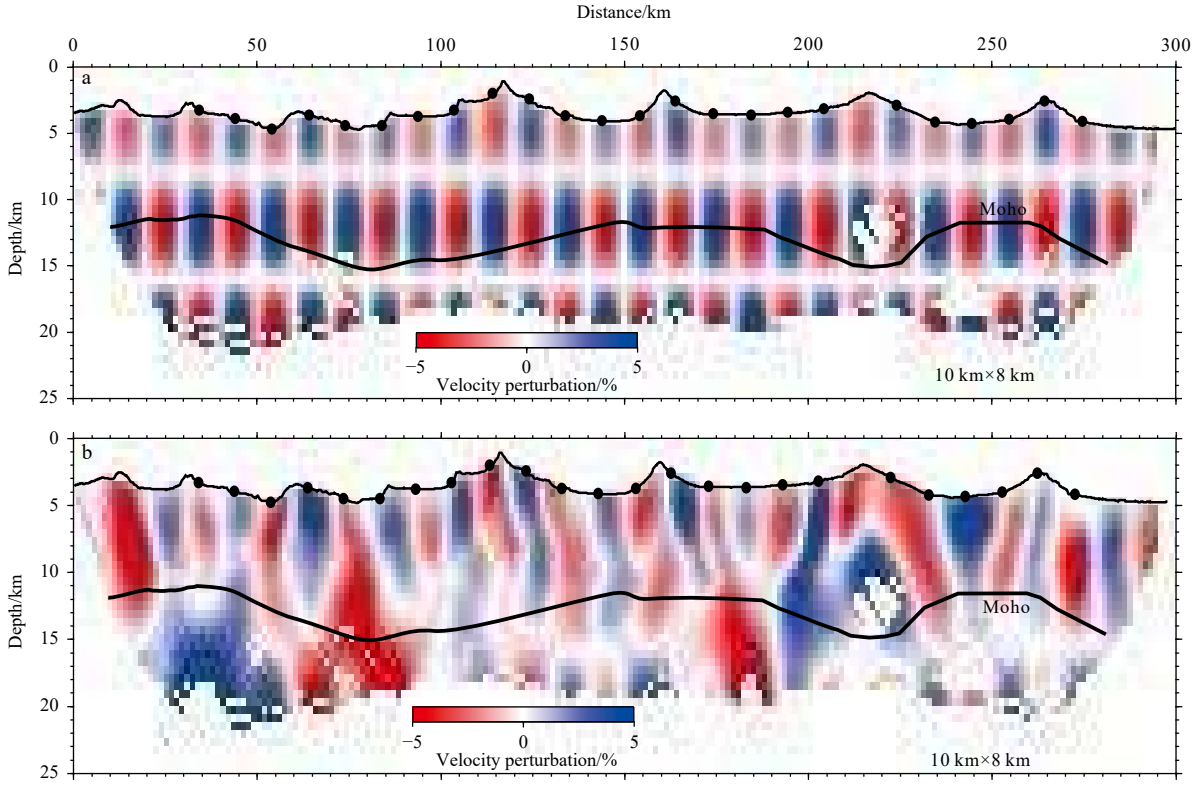

Fig. 4. Checkerboard resolution test results of the profile KPR2020-3 (a), and input velocity perturbation of 5% with the cell of 10 km× 8 km (b). Recovered velocity perturbations from the checkerboard tests and the perturbed dimensions is 10 km×8 km.

in crustal thickness and Moho depth along the profile (Fig. 3b). Along the profile, the thickness of the sedimentary layer is relatively thin, or even missing above the seamounts, with velocity increasing rapidly from 2.0 km/s to 4.0 km/s. Beneath the sedimentary layer, the top of the crust has a velocity of 4.0 km/s, and increases to 7.0 km/s in the bottom, with a crustal thickness of 6–12 km. The upper and lower crusts are defined based on the significant change in velocity gradient at the boundary, which is consist to the isovelocity contour of 6.4 km/s. The upper crust has a high velocity gradient (~1 s^{-1}) and the thickness is between 2 km and 4 km, while the lower crust has a lower-velocity gradient (<0.2 s^{-1}), and is characterized by a substantial lateral variation both in crustal thickness and velocity. High (~7.2 km/s) and low (~6.7 km/s) velocity anomalies are revealed in the lower crust below seamounts.

The Moho is located at a depth between 11 km and 16 km along the profile. It is constrained by the PmP phases in part of our final velocity model, while other parts are consistent with the 7.0 km/s isovelocity contour (Fig. 3b). Velocities in upper mantle are about 7.2–7.6 km/s and markedly less than normal upper mantle P-wave velocity (V_p) of 8.0 km/s. The low velocity in upper mantle beneath the arc is also reported in IBM arc, and the slow mantle velocities beneath the arc indicate the existence of the transformation of the crustal materials, which is accompanied with the crustal growth (Takahashi et al., 2008, 2009).

5 Discussion

5.1 *Crust nature of the southern part of the KPR*

Crustal structure is crucial to understand the nature of the KPR. Based on 27 OBS profiles across the KPR, Nishizawa et al. (2007) discussed the crustal variations of the KPR between 15°N and 21°N, and compared it with crustal structure of the conjugate IBM arc. They suggested that KPR had a crust thickness of 8–23 km, with a 5-km middle crust (velocity of 6.0–6.8 km/s) and low velocity anomaly in the upper mantle. Therefore, the KPR is considered to be a mature island arc as IBM arc. However, other studies based on joint gravity-magmatic-seismic conversion argued that the KPR is lack of middle crust and the crustal thickness is relatively thinner than the IBM arc (Zhang et al., 2012, 2018). Comparison of the 1D velocity among the KPR, IBM and mature island arc also showed that KRP had a thinner thickness and higher velocity than that of the IBM and mature island arc (Calvert, 2011). The crustal nature of the KPR is still in debated.

Typical oceanic crust can be divided into Layer 2 (upper crust) and Layer 3 (lower crust) (White, 1984; White et al., 1984). Layer 2 is usually 2–3 km thick and shows a high velocity gradient with depth, ranging from about 4.0 km/s to 6.4 km/s, while the Layer 3 is about 5 km thick with a low velocity gradient of 0.1–0.2 s^{-1} or less (White, 1984; White et al., 1984).

While for mature island arc, it is generally characterized by (1) a crustal thickness of ~20 km; (2) a 3–13 km thick middle crust with velocity of 6.4–6.8 km/s; (3) a deep reflector with velocity lower than 8.0 km/s in the upper mantle; and (4) high and low velocity anomalies in the lower crust (Nishizawa et al., 2007; Takahashi et al., 2008, 2009; Kodaira et al., 2007a, b).

The 10-km interval profile KPR2020-3 gives an opportunity to unveil the detailed crustal structure of the southern KPR, as well as the crustal nature. The crustal thickness along profile KPR2020-3 is about 6–12 km with the upper and lower crust velocities of 4.0–6.4 km/s and 6.4–7.0 km/s, respectively. It is slightly thicker than normal oceanic crust, but is much thinner than mature island crust such as the IBM arc. Neither middle crust nor deep reflector in the upper mantle was identified in the southern part of the KPR. Although crustal thickness is slightly thicker than that of the typical oceanic crust, either velocity structure or gradient in this study indicates that at least the southern part of the KPR is of oceanic crust nature.

This study also applied 1D velocity model for different position of KPR2020-3. All velocity curves show a sharp increase to ~6.4 km/s. With comparison with typical oceanic crust, continental crust, and island arc crust (e.g., IBM arc, Calvert, 2011), the southern part of KPR has much higher velocity gradient above Moho than the mature arc or continental crust, but is similar to that of oceanic crust. Comparison of the 1D velocity among the KPR, IBM arc crust and continental crust showed that the KRP had a thinner thickness and higher velocity than those of the IBM arc, or mature island arc (Fig. 5). These imply that the crust structure of the south KPR is quite different from the north. Therefore, this study suggests that the southern part of the KPR is a thicken oceanic crust rather than an island arc one. The velocity anomalies in the lower crust and upper mantle imply a transition stage from oceanic crust to island arc one.

5.2 *Velocity anomaly and crust evolution*

Our velocity model suggests that the seamount edifices contain high and low velocity anomaly in the lower crust. The velocity anomalies in the lower crust below the seamount are also discovered in the fossil spreading center, such as the South China Sea (Zhang et al., 2020), which was interpreted as episodic magmatic intrusion; or subduction-related arcs, such as the IBM (Suyehiro et al., 1996; Takahashi et al., 2009) and Aleutian arc (Holbrook et al., 1999), which was related to partial melting due to crustal extension or remains of arc magmatism (high velocity anomaly), and crustal differentiation promoted by back-arc opening (low velocity anomaly) (Takahashi et al., 2008, 2009).

Velocity anomaly is considered to be a key to understand the crustal growth, as the low velocity (LV) in the lower crust and upper mantle beneath the arc regions probably indicate the existence of the transformation of the crustal materials (Takahashi et al., 2009). LV in the lower crust might originate from melting (Dunn et al., 2005; Canales et al., 2007; Zhao et al., 2012) and crustal differentiation (Jull and Kelemen, 2001; Takahashi et al., 2008; Kodaira et al., 2007b). Magma chamber or melting caused by robust magma supply in the lower crust could produce LV. However, prolonged magma cooling could consolidate the melting, which is manifested as high velocity in the lower crust. Previous studies on numerical modeling showed that the cooling time of magma has an important relationship with the volume of magma intrusion, and the melts with a radius of 3–6 km and a height of 3.7–9.2 km needs 10 Ma to completely cooling and consolidation (Tang et al., 2013). $^{40}Ar/^{39}Ar$ dating ages of rock samples from the seamounts of the KPR are mainly at 30–25 Ma, but some are as young as 22 Ma (Ishizuka et al. 2011). This represents the final stage of the KPR volcanism. Therefore, the 12 km ×8 km low velocity anomalies of this study could not be originated from the magma melts. Differentiated basaltic magma in the lower crust is related to mafic to ultramafic crustal component transformation to upper mantle, which lead to inhomogenous velocity anomalies and crust evolution (Tatsumi et al., 2008; Takahashi et al., 2008, 2009). Jull and Kelemen (2001) indicated that the lower crustal materials might sink into the mantle because these have higher density than mantle olivine, which might be a part of the transformation and crustal growth. Downward transfer of dense crustal materials into mantle can lead to slow upper mantle V_p and LV in the lower crust (Takahashi et al., 2009). The similar velocity anomalies detected in this study might also indicate a crustal differentiation process (Fig. 6), suggesting advanced crustal differentiation and evolution.

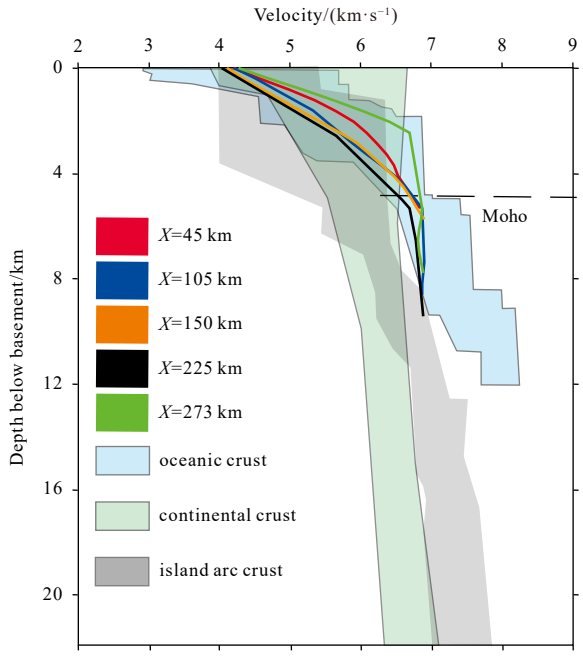

Fig. 5. 1D velocity-depth profiles extracted from the velocity model. The oceanic crust velocities are obtained from White (1992). The continental crust velocities are referenced from Christensen and Mooney (1995). The island arc crust is obtained from Calvert (2011) and Takahashi et al. (2008, 2009). *X* represents the positions (distance axis) in the Fig. 3

High velocity (HV) in the lower crust is usually originated from serpentinized peridotites (Whitmarsh et al., 1993, 2001; Reston, 2009; Franke, 2013), magmatic underplating (Yan et al., 2001; Wang et al., 2006; Wei et al., 2011; Wan et al., 2017), or remnant arcs magmatism (Suyehiro et al., 1996; Takahashi et al., 2008, 2009; Calvert, 2011; Holbrook et al., 1999; Wan et al., 2017). Serpentinization usually occurs at the extremely stretched margins or mid-ocean ridge, and is generally interpreted as the result of the interaction of mantle peridotites with seawater through faults linking the shallow upper mantle with the seafloor (Whitmarsh et al., 2001; Reston, 2009). In our models, velocity anomalies are only distributed in the lower crust but not the whole crust, implying no crust-scale normal faulting occurs here to bring seawater into mantle. Furthermore, Louden and Chian (1999) proposed that although serpentinization of the upper mantle could cause HV in the lower crust, no PmP phases can be generated since the Moho is more like a velocity transition zone than an interface. This study observed clear PmP reflections from the bottom of HV lower crust beneath the KRP. Thus, a serpentinized mantle origin may be excluded.

Another possible origin of the HV in the lower crust is magmatic activities. Zhang et al. (2020) compiled the seamounts structures and then gave models of seamount formation and magmatism duration. They proposed that numbers of seamounts and the crustal thickness are related to episodic magmatism with different origin. The ages of OIB-type basaltic samples of KPR are between 48 Ma and 25 Ma (Ishizuka et al., 2011). The former is in consistent with the initial subduction of the Pacific plate beneath the West Philippine Basin, and the latter is fit with seafloor spreading in the Shikoku Basin and Parece Vela Basin. Thus, the HV in our models might be both influenced by the early-stage subduction-related arc magmatism and the later-stage seafloor spreading magmatism. The velocity structure shows that seamounts above HV1 (~120 km, Fig. 6) are characterized by the existence of two summits with thick crust, indicating multi-stage

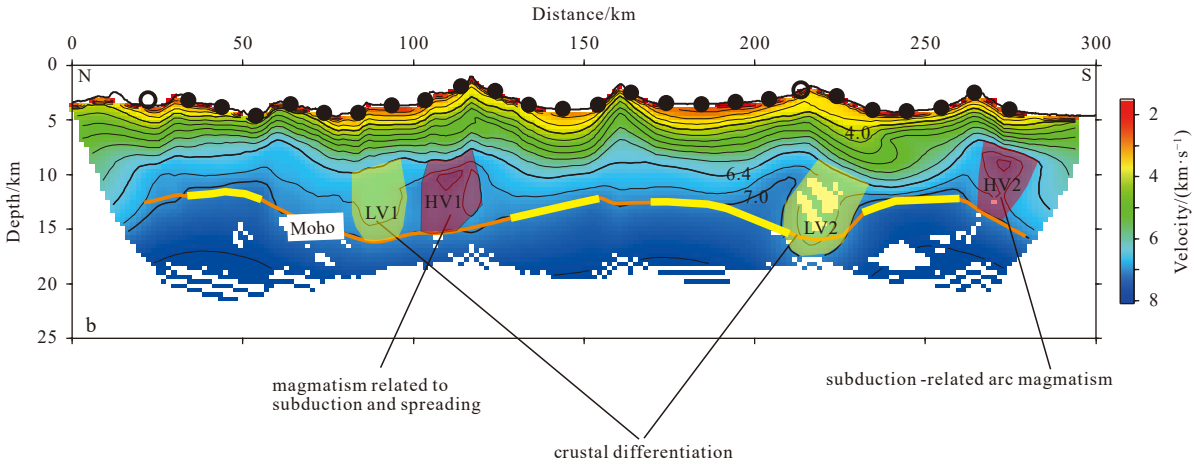

Fig. 6. Schematic with interpretation about the velocity anomaly and crust evolution of the southern part of the KPR (modified from Takahashi et al., 2008)

magmatism. While the seamount above HV2 (~280 km, Fig.6) has only one summit at the igneous basement, and the crust thickness is much thinner (~7 km), implying a stable volcanic source. The age of the rock samples from the seamount above HV2 is about 32 Ma (Ishizuka et al., 2011), which is earlier than the back-arc spreading in Parece Vela Basin. The formation might be related with the subduction-related magmatism. In summary, the HV1 is a product of a combination of subduction-related arc magmatism and spreading-related one. In contrast, HV2 was affected by subduction-related arc magmatism (Fig. 6).

6 Conclusion

Crustal structure imaged from wide-angle seismic OBS data along the profile KRP2020-3 in the southern part of the KPR is presented and compared the velocity characteristics with those of the typical oceanic crust and mature arc crust. This study finds that the crustal thickness of KPR2020-3 is 6–12 km with velocity of 4.0 km/s to 7.0 km/s, and the velocity gradients in the upper and lower crusts are similar to that of the typical oceanic crust, implying the southern part of the KPR is a thicken oceanic crust rather than mature arc crust. LVs in the lower crust and upper mantle reveled by KPR2020-3 are explained by crustal differentiation, which implies advanced crustal evolution from normal oceanic crust to partly thicken oceanic crust. According to dating ages of rock samples from the seamounts of the KPR and seamount formation models, the HV1 in the lower crust is a product of a combination of magmatism related to subduction and spreading, while the HV2 is originated from the magmatism related to subduction.

Acknowledgments

We thank all the scientists and crew of the R/V *Dayanghao* for assisting in collecting the field data during the cruise. Some of our figures were plotted using Generic Mapping Tools (Wessel and Smith, 1995).

References

Arculus R J, Ishizuka O, Bogus K A, et al. 2015. A record of spontaneous subduction initiation in the Izu-Bonin-Mariana arc. Nature Geoscience, 8(9): 728–733, doi: 10.1038/ngeo2515

Calvert A J. 2011. The seismic structure of island arc crust. In: Brown D, Ryan P D, eds. Arc-Continent Collision. Berlin, Heidelberg: Springer, 87–119

Canales J P, Sohn R A, deMartin B J. 2007. Crustal structure of the Trans-Atlantic Geotraverse (TAG) segment (Mid-Atlantic Ridge, 26°10′N): implications for the nature of hydrothermal circulation and detachment faulting at slow spreading ridges. Geochemistry, Geophysics, Geosystems, 8(8): Q08004, doi: 10.1029/2007GC001629

Christensen N I, Mooney W D. 1995. Seismic velocity structure and composition of the continental crust: a global view. Journal of Geophysical Research: Solid Earth, 100(B6): 9761–9788, doi: 10.1029/95JB00259

Cosca M, Arculus R, Pearce J. 1998. $^{40}Ar/^{39}Ar$ and K-Ar geochronological age constraints for the inception and early evolution of the Izu-Bonin-Mariana arc system. Island Arc, 7(3): 579–595, doi: 10.1111/j.1440-1738.1998.00211.x

Deschamps A, Lallemand S. 2002. The West Philippine Basin: an Eocene to early Oligocene back arc basin opened between two opposed subduction zones. Journal of Geophysical Research: Solid Earth, 107(B12): 2322, doi: 10.1029/2001JB001706

Dunn R A, Lekić V, Detrick R S, et al. 2005. Three-dimensional seismic structure of the Mid-Atlantic Ridge (35°N): evidence for focused melt supply and lower crustal dike injection. Journal of Geophysical Research: Solid Earth, 110(B9): B09101, doi: 10.1029/2004JB003473

Franke D. 2013. Rifting, lithosphere breakup and volcanism: comparison of magma-poor and volcanic rifted margins. Marine and Petroleum Geology, 43: 63–87, doi: 10.1016/j.marpetgeo.2012.11.003

Hall R. 2002. Cenozoic geological and plate tectonic evolution of SE Asia and the SW Pacific: computer-based reconstructions, model and animations. Journal of Asian Earth Sciences, 20(4): 353–431, doi: 10.1016/S1367-9120(01)00069-4

Hilde T W C, Lee C S. 1984. Origin and evolution of the West Philippine Basin: a new interpretation. Tectonophysics, 102(1–4): 85–104, doi: 10.1016/0040-1951(84)90009-X

Holbrook W S, Lizarralde D, McGeary S, et al. 1999. Structure and composition of the Aleutian island arc and implications for continental crustal growth. Geology, 27(1): 31–34, doi: 10.1130/0091-7613(1999)027<0031:SACOTA>2.3.CO;2

Ishizuka O, Hickey-Vargas R, Arculus R J, et al. 2018. Age of Izu–Bonin–Mariana arc basement. Earth and Planetary Science Letters, 481: 80–90, doi: 10.1016/j.epsl.2017.10.023

Ishizuka O, Taylor R N, Yuasa M, et al. 2011. Making and breaking an island arc: a new perspective from the Oligocene Kyushu-Palau arc, Philippine Sea. Geochemistry, Geophysics, Geosystems, 12(5): Q05005, doi: 10.1029/2010GC003440

Jull M, Kelemen P B. 2001. On the conditions for lower crustal convective instability. Journal of Geophysical Research: Solid Earth, 106(B4): 6423–6446, doi: 10.1029/2000JB900357

Kodaira S, Sato T, Takahashi N, et al. 2007a. New seismological constraints on growth of continental crust in the Izu-Bonin intra-

oceanic arc. Geology, 35(11): 1031–1034, doi: 10.1130/G23901A.1
Kodaira S, Sato T, Takahashi N, et al. 2007b. Seismological evidence for variable growth of crust along the Izu intraoceanic arc. Journal of Geophysical Research: Solid Earth, 112(B5): B05104
Korenaga J, Holbrook W S, Kent G M, et al. 2000. Crustal structure of the southeast Greenland margin from joint refraction and reflection seismic tomography. Journal of Geophysical Research: Solid Earth, 105(B9): 21591–21614, doi: 10.1029/2000JB900188
Leng W, Gurnis M. 2015. Subduction initiation at relic arcs. Geophysical Research Letters, 42(17): 7014–7021, doi: 10.1002/2015GL064985
Louden K E, Chian D, 1999. The deep structure of non-volcanic rifted continental margins. The Royal Society, 357: 767–805
Nishizawa A, Kaneda K, Katagiri Y, et al. 2007. Variation in crustal structure along the Kyushu-Palau Ridge at 15-21°N on the Philippine Sea plate based on seismic refraction profiles. Earth, Planets and Space, 59(6): e17–e20
Nishizawa A, Kaneda K, Oikawa M. 2016. Crust and uppermost mantle structure of the Kyushu-Palau Ridge, remnant arc on the Philippine Sea plate. Earth, Planets and Space, 68(1): 30, doi: 10.1186/s40623-016-0407-3
Okino K, Kasuga S, Ohara Y. 1998. A new scenario of the Parece Vela Basin genesis. Marine Geophysical Research, 20(1): 21–40, doi: 10.1023/A:1004377422118
Okino Y, Shimakawa Y, Nagaoka S. 1994. Evolution of the Shikoku Basin. Journal of Geomagnetism and Geoelectricity, 46(6): 463–479, doi: 10.5636/jgg.46.463
Reston T J. 2009. The structure, evolution and symmetry of the magma-poor rifted margins of the North and Central Atlantic: a synthesis. Tectonophysics, 468(1–4): 6–27, doi: 10.1016/j.tecto.2008.09.002
Sdrolias M, Müller R D. 2006. Controls on back-arc basin formation. Geochemistry, Geophysics, Geosystems, 7(4): Q04016, doi: 10.1029/2005GC001090
Stern R J. 2004. Subduction initiation: spontaneous and induced. Earth and Planetary Science Letters, 226(3–4): 275–292, doi: 10.1016/S0012-821X(04)00498-4
Stern R J, Gerya T. 2018. Subduction initiation in nature and models: a review. Tectonophysics, 746: 173–198, doi: 10.1016/j.tecto.2017.10.014
Suyehiro K, Takahashi N, Ariie Y, et al. 1996. Continental crust, crustal underplating, and low-*Q* upper mantle beneath an oceanic island arc. Science, 272(5260): 390–392, doi: 10.1126/science.272.5260.390
Takahashi N, Kodaira S, Tatsumi Y, et al. 2008. Structure and growth of the Izu-Bonin-Mariana arc crust: 1. Seismic constraint on crust and mantle structure of the Mariana arc–back-arc system. Journal of Geophysical Research: Solid Earth, 113(B1): B01104, doi: 10.1029/2007JB005120
Takahashi N, Kodaira S, Tatsumi Y, et al. 2009. Structural variations of arc crusts and rifted margins in the southern Izu-Ogasawara arc-back arc system. Geochemistry, Geophysics, Geosystems, 10(9): Q09X08, doi: 10.1029/2008GC002146
Tang Xiaoyin, Zhang Gongcheng, Liang Jianshe, et al. 2013. Influence of igneous intrusions on the temperature field and organic maturity of the Changchang Sag, Qiongdongnan Basin, South China Sea. Chinese Journal of Geophysics, 56(1): 159–169
Tatsumi Y, Shukuno H, Tani K, et al. 2008. Structure and growth of the Izu-Bonin-Mariana arc crust: 2. Role of crust-mantle transformation and the transparent Moho in arc crust evolution. Journal of Geophysical Research: Solid Earth, 113(B2): B02203, doi: 10.1029/2007JB005121
Wan Kuiyuan, Xia Shaohong, Cao Jinghe, et al. 2017. Deep seismic structure of the northeastern South China Sea: origin of a high-velocity layer in the lower crust. Journal of Geophysical Research: Solid Earth, 122(4): 2831–2858, doi: 10.1002/2016JB013481
Wang T K, Chen M K, Lee C S, et al. 2006. Seismic imaging of the transitional crust across the northeastern margin of the South China Sea. Tectonophysics, 412(3–4): 237–254, doi: 10.1016/j.tecto.2005.10.039
Watts A B, Weissel J K. 1975. Tectonic history of the Shikoku marginal basin. Earth and Planetary Science Letters, 25(3): 239–250, doi: 10.1016/0012-821X(75)90238-1
Wei Xiaodong, Ding Weiwei, Christeson G L, et al. 2021. Mesozoic suture zone in the East China Sea: evidence from wide-angle seismic profiles. Tectonophysics, 820: 229116, doi: 10.1016/j.tecto.2021.229116
Wei Xiaodong, Ruan Aiguo, Zhao Minghui, et al. 2011. A wide-angle Obs profile across the Dongsha Uplift and Chaoshan Depression in the Mid-Northern South China Sea. Chinese Journal of Geophysics, 54(6): 1149–1160, doi: 10.1002/cjg2.1691
White R S. 1984. Atlantic oceanic crust: seismic structure of a slow-spreading ridge. Geological Society, London, Special Publications, 13(1): 101–111
White R S. 1992. Crustal structure and magmatism of North Atlantic continental margins. Journal of the Geological Society, 149(5): 841–854, doi: 10.1144/gsjgs.149.5.0841
White R S, Detrick R S, Sinha M C, et al. 1984. Anomalous seismic crustal structure of oceanic fracture zones. Geophysical Journal International, 79(3): 779–798, doi: 10.1111/j.1365-246X.1984.tb02868.x
Whitmarsh R B, Manatschal G, Minshull T A. 2001. Evolution of magma-poor continental margins from rifting to seafloor spreading. Nature, 413(6852): 150–154, doi: 10.1038/35093085
Whitmarsh R B, Pinheiro L M, Miles P R, et al. 1993. Thin crust at the western Iberia Ocean-Continent transition and ophiolites. Tectonics, 12(5): 1230–1239, doi: 10.1029/93TC00059
Yamazaki T, Seama K, Okino K, et al. 2003. Spreading process of the northern Mariana Trough: rifting-spreading transition at 22°N. Geochemistry, Geophysics, Geosystems, 4(9): 1075, doi: 10.1029/2002GC000492
Yan Pin, Zhou Di, Liu Zhaoshu. 2001. A crustal structure profile across the northern continental margin of the South China Sea. Tectonophysics, 338(1): 1–21, doi: 10.1016/S0040-1951(01)00062-2
Zelt C, Forsyth D, 1994. Modeling wide-angle seismic data for crustal structure: Southeastern Grenville Province. Journal of Geophysical Research: Solid Earth, 99 (11), 11687–11704, doi: 10.1029/93JB02764
Zhang Zhengyi, Fan Jianke, Bai Yongliang, et al. 2018. Joint inversion of gravity-magnetic-seismic data of a typical profile in the China Sea-Western Pacific area. Chinese Journal of Geophysics, 61(7): 2871–2891
Zhang Jie, Li Jiabiao, Ding Weiwei. 2012. Reviews of the study on crustal structure and evolution of the Kyushu-Palau Ridge. Advances in Marine Science, 30(4): 595–607
Zhang Jie, Li Jiabiao, Ruan Aiguo, et al. 2020. Seismic structure of a postspreading seamount emplaced on the fossil spreading center in the Southwest Subbasin of the South China Sea. Journal of Geophysical Research: Solid Earth, 125(10): e2020JB019827, doi: 10.1029/2020JB019827
Zhao Minghui, Canales J P, Sohn R A. 2012. Three-dimensional seismic structure of a Mid-Atlantic Ridge segment characterized by active detachment faulting (Trans-Atlantic Geotraverse, 25°55′N-26°20′N). Geochemistry, Geophysics, Geosystems, 13(11): Q0AG13, doi: 10.1029/2012GC004454